MATEC Web of Conferences **14**, 12001 (2014)
DOI: 10.1051/matecconf/20141412001
© Owned by the authors, published by EDP Sciences, 2014

Multipass forging of Inconel 718 in the delta-Supersolvus domain: assessing and modeling microstructure evolution

Meriem Zouari[1,2,a], Roland E. Loge[2,3], Oscar Beltran[2], Sébastien Rousselle[1,2], and Nathalie Bozzolo[2]

[1] Manoir Aerospace-Forges de Bologne SAS, 52905 Chaumont, France
[2] MINES ParisTech, CEMEF – Centre de mise en forme des matériaux, CNRS UMR 7635, CS 10207 rue Claude Daunesse, 06904 Sophia Antipolis Cedex, France
[3] Thermomechanical Metallurgy Laboratory – PX Group Chair, Ecole Polytechnique Fédérale de Lausanne (EPFL), Rue de la Maladière 71B – CP 526, 2002 Neuchâtel, Switzerland

Abstract. This work is focused on the evolution of the microstructure of Inconel 718 during multi-pass forging processes. During the forming process, the material is subjected to several physical phenomena such as work-hardening, recovery, recrystallization and grain growth. In this work, transformation kinetics are modeled in the δ-Supersolvus domain (T>Tsolvus) where the alloy is single-phase, all the alloying elements being dissolved into the FCC matrix. Torsion tests were used to simulate the forging process and recrystallization kinetics was modeled using a discontinuous dynamic recrystallization (DDRX) two-site mean field model. The microstructure evolution under hot forging conditions is predicted in both dynamic and post-dynamic regimes based on the initial distribution of grain size and the evolution of dislocation density distribution during each step of the process. The model predicts recrystallization kinetics, recrystallized grain size distribution and stress–strain curve for different thermo-mechanical conditions and makes the connection between dynamic and post-dynamic regimes.

1. Introduction

Inconel 718 is a nickel-based superalloy combining good mechanical properties and resistance to oxidation at high temperatures. This alloy is widely used for manufacturing hot parts of turbojet engines. During hot forging of these parts, the microstructure of the alloy changes with the different cycles of heating, holding at high temperature, forging and cooling. The properties of the final piece depend greatly on the microstructure obtained at the end of the forging process. Controlling the final grain size is a key element to improve the mechanical properties of the forged pieces and hence meet the tight specifications imposed by the aeronautic industry. During the forming process, the material is subjected to several physical phenomena such as work-hardening, recovery, discontinuous recrystallization and grain growth.

The recrystallization kinetics of Inconel 718 has been extensively studied using hot compression, high temperature rolling and torsion tests [1–6]. Few numerical models simulating recrystallization kinetics in Inconel 718 can be found in the literature. *Park et al.* used finite element method (FEM) simulations to model multi-pass forging of Inconel 718 [8]. *De Jaeger et al.* proposed a 3D cellular automaton model to simulate single and multi-pass hot forging of Inconel 718 [9]. Because of the need of an explicit representation of microstructures and a statistical number of grains, these approaches have as a consequence a high computational cost. However, from an industrial perspective, the aim is to have a relatively simple model relating the microstructure to the processing parameters without being computationally demanding.

In this study, static, dynamic and post-dynamic evolutions during the forging process are modeled in the δ-Supersolvus domain by a 2-site mean field approach [7] which is much less demanding from a computation time point of view. The kinetics of recrystallization and stress–strain curves are predicted for different thermomechanical conditions and a connection is made between dynamic and post-dynamic regimes, which is usually difficult to do with more phenomenological approaches.

2. Material and experimental procedure

Isothermal torsion tests were performed at constant strain rate to study both dynamic and post-dynamic recrystallization for different thermomechanical conditions. Torsion specimens were machined from a 150 mm diameter billet having the chemical composition given in Table 1. The samples were solution annealed at 1050 °C for 60 minutes before deformation in order to dissolve all the alloying elements into the FCC matrix. The grain size after the solution annealing treatment reached 90 microns and the microstructure was single phased (except for the presence of few carbides, which will be ignored in the following).

Two experimental procedures were investigated. In the first one, samples were held at high temperature, then deformed at a given strain rate up to different strains,

[a] Corresponding author: meriem.zouari@mines-paristech.fr

This is an Open Access article distributed under the terms of the Creative Commons Attribution License 4.0, which permits unrestricted use, distribution, and reproduction in any medium, provided the original work is properly cited.

Table 1. Composition of the studied material (wt%).

Ni	Fe	Cr	Nb	Mo	Ti,Al,Co	Autres
54.39	17.78	17.25	5.37	2.9	<1	<0.1

and then quenched immediately in water to investigate recrystallization during the dynamic regime. In the second one, the samples were kept at high temperature for different times after deformation and then quenched in water to study recrystallization during the post-dynamic regime. Each sample was then cut and mechanically polished. Oxide Polishing Suspension (OPS) was used to perform a mechanical-chemical polishing and reveal the microstructure.

Finally, the microstructure of each sample was characterized using the Electron Back Scattered Electron Diffraction (EBSD) technique coupled to a Field Emission Gun Scanning Electron Microscope (Zeiss SUPRA40 FEGSEM). EBSD maps were acquired using a Bruker Crystalign system operated at a step size between 0.2 μm and 0.8 μm; they were analyzed using the OIM^{TM}Data Analysis software. Grains were identified in EBSD maps as groups of (at least 2) neighboring pixels misoriented by less than 5°.

3. Physical mechanisms and modelling

Recrystallization kinetics was modeled using a discontinuous dynamic recrystallization (DDRX) two-site mean field model [7]. This model was first used to model the recrystallization kinetics of a 304L austenitic stainless steel. In this work, the model is adapted to Inconel 718 which is also a low stacking fault energy material, and has therefore a similar behavior as 304L steel.

3.1. Early stages of recrystallization

In the dynamic regime, as the material deforms, the dislocation density increases progressively. Locally, along some grain boundaries, the dislocation density reaches a critical value ρ_{cr} and new dislocation-free grains nucleate (Fig. 1). The evolution of dislocation density in a grain is calculated based on the Yoshie–Lasraoui–Jonas hardening law [10]:

$$\frac{\partial \rho}{\partial t} = \left[K_1\left(\dot{\varepsilon}\right) - K_2\left(\dot{\varepsilon}, \mathrm{T}\right), \rho\right].\dot{\varepsilon} \qquad (1)$$

where ρ is the grain average dislocation density, $\dot{\varepsilon}$ the strain rate, K_1 the hardening parameter and K_2 the dynamic recovery parameter. This model assumes that hardening depends only on strain rate and that dynamic recovery depends on both strain rate and temperature.

At the early stages of recrystallization, the microstructure consists in two types of grains: long deformed grains and small equiaxed recrystallized grains on the boundaries of the most deformed grains (Fig. 1). Further nucleation and growth of new recrystallized grains lead to necklace type microstructures (Fig. 2).

In the model and for the sake of simplification, the microstructure is represented by a set of spherical grains with known initial distributions of diameters

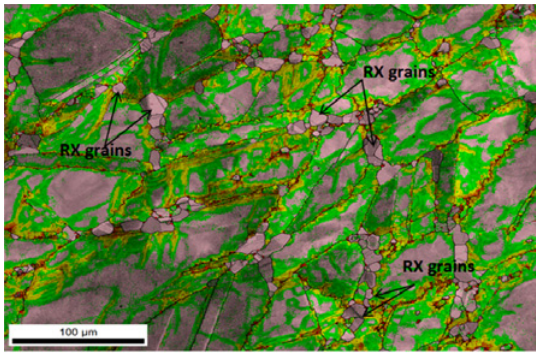

Figure 1. Kernel Average Misorientation map showing newly nucleated grains at the boundaries of deformed grains.

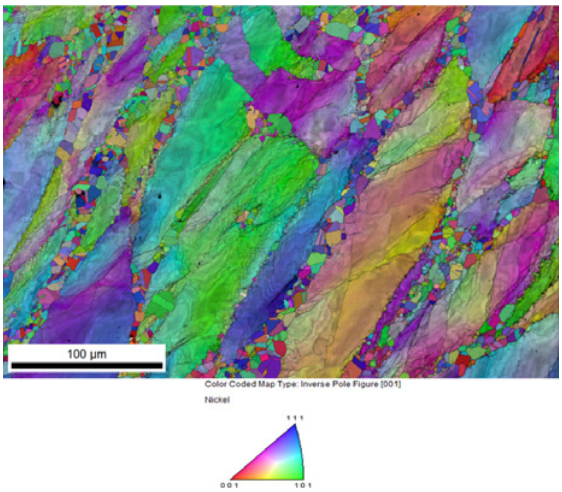

Figure 2. Necklace structure observed at the beginning of recrystallization.

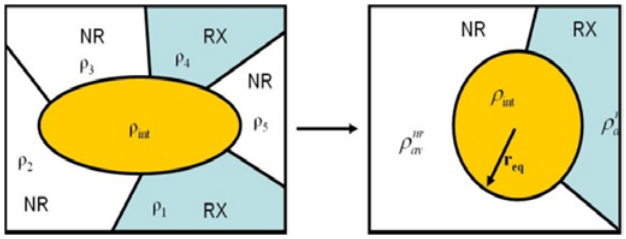

Figure 3. Schematic representations of a partially recrystallized microstructure (left) defining the two considered HEM surrounding a category of grains (right) [7].

and dislocation density. For each grain category, the neighborhood is represented by two Homogeneous Equivalent Media (HEM): NR and RX, respectively representative of the non-recrystallized and recrystallized populations of grains. Each HEM is represented by an average dislocation density ρ_{av}^{HEM} and an average grain size r_{av}^{HEM} (Fig. 3).

Each representative grain interacts with the two surrounding media. The volume change of recrystallized and non-recrystallized media controls the evolution of the microstructure.

The nucleation rate is calculated based on the following equation:

$$\dot{N}_{i,nucl} = K_g(\dot{\varepsilon}, T) S_{cr} \frac{N_i r_i^q (\rho_i - \rho_{cr})^{bg}}{\sum_{p_k > p_{cr}} N_k r_k^q (\rho_k - \rho_{cr})^{bg}} \quad (2)$$

where K_g is the nucleation parameter and S_{cr} the total surface area of grains with a dislocation density higher than ρ_{cr}. r_i, ρ_{cr} and N_i are respectively the radius, the dislocation density and the number of grains associated to a given representative grain i. bg is a constant set to 3 and q is a constant set to 2 in the case of necklace-type nucleation [7].

3.2. Recrystallization progress

As deformation continues, the fraction of recrystallized grain increases by both the nucleation of new grains and the growth of previously nucleated grains.

The migration of grain boundaries is controlled by two forces: the capillarity force related to the curvature of gain boundaries (Hillert model [11]) and the force related to the distribution of stored energy (difference of dislocation density across boundaries). The velocity of grain boundaries is given by the following equation:

$$v = M(\dot{\varepsilon}, T) . \left[\tau(\rho - \bar{\rho}) + \gamma \left(\frac{1}{R} - \frac{1}{\bar{R}} \right) \right] . \quad (3)$$

where M is the grain boundary mobility, ρ and R the dislocation density and grain radius of the considered grain category, $\bar{\rho}$ and $\bar{R}$ the average dislocation density and radius in the considered HEM, γ the grain boundary energy and τ the energy per unit dislocation length.

A parameter $K_3 = M.\tau$ is introduced in the model, so that Eq. (3) becomes:

$$v = K_3(\dot{\varepsilon}, T) . \left[(\rho - \bar{\rho}) + \frac{\gamma}{\tau} \left(\frac{1}{R} - \frac{1}{\bar{R}} \right) \right] . \quad (4)$$

When the dislocation density is higher than ρ_{cr}, a new recrystallized grain is nucleated with a size r_u and a dislocation density ρ_0. The nucleus size r_u is given by:

$$r_u = \frac{2\gamma}{\tau \rho_c} . \quad (5)$$

The critical dislocation density is calculated based on Eqs. (1), (4) and (5) and is given by:

$$\rho_{cr} = \left[\frac{\frac{-4K_2 \dot{\varepsilon} \gamma}{K_3 \tau}}{Ln(1 - \frac{K_2}{K_3} \rho_{cr})} \right]^{\frac{1}{2}} . \quad (6)$$

An iterative procedure is used to solve the equation (6) and calculate the value of ρ_{cr}. As it can be observed from Eqs. (5) and (6), both the critical density and the nucleus size depend on the applied thermomechanical conditions through the strain rate and the parameters K_1, K_2 and K_3.

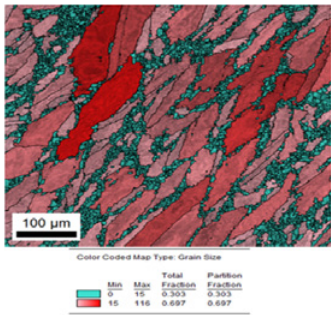

Figure 4. Identification of recrystallized grains based on the size criterion.

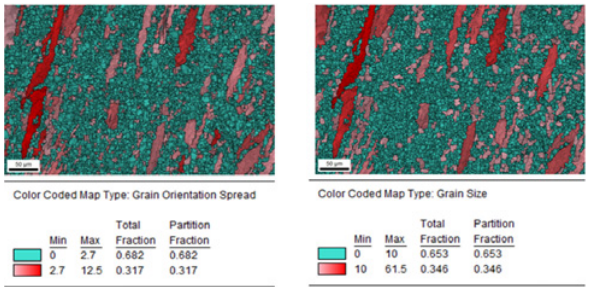

Figure 5. Identification of recrystallized grains a) based on grain size (RX size $<10\,\mu$m, X = 68%), b) based on the grain orientation spread criteria (GOS(RX grains) <2.7, X = 65%).

3.3. End of recrystallization

During hot deformation, recrystallized grains grow at the expense of old deformed grains as a consequence of stored energy difference. As the material becomes almost 100% recrystallized, RX and NR grains reach a similar size. Consequently, at this stage, the recrystallized grains are experimentally much more difficult to identify.

At the first stages of deformation, the recrystallized grains can easily be identified by i) their small size compared to the initial grain structure (provided that the initial grain size was significantly larger than the recrystallized grain size) and ii) their equiaxed shape (Fig. 4).

Using an intragranular misorientation criterion is an alternative method very much used in static recrystallization studies.

Using the OIM software, the grain orientation spread (G.O.S) can be used for example as a measurement of the intragranular misorientations. GOS is a grain property, calculated as the average misorientation angle between each point of a grain and the average orientation of the grain. Grains with higher dislocation densities have higher GOS.

Under dynamic conditions, the early recrystallized grains are subsequently deformed so that their dislocation density can become close to the NR dislocation density. Nevertheless, comparing the results based on a grain size criterion and on a GOS criterion enables to have a better estimation of recrystallized grains (Fig. 5).

After a certain amount of deformation, the material is fully recrystallized. The RX grain size stabilizes and a flow stress steady state is reached. Accordingly, the average dislocation density of RX grains reaches a constant value.

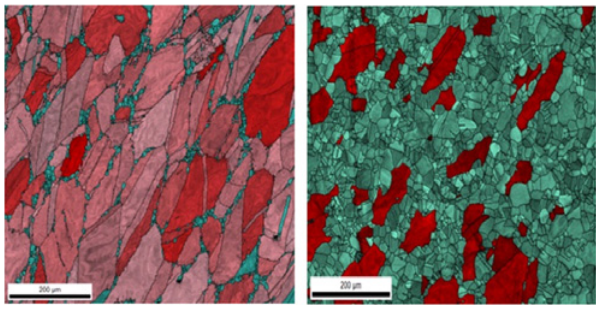

Figure 6. Post-dynamic evolution at 1020 °C in a partially recrystallized sample a) immediately quenched b) after holding for 60s at 1020C (NR grains appear in red).

3.4. Post-dynamic evolution

From an industrial point of view, the microstructure evolution right after deformation, before and during cooling can not be avoided due to the thermal inertia of the pieces. If during the forming process the applied deformation does not allow to dynamically achieve full recrystallization, already formed nuclei may grow after deformation has been stopped, leading to the so-called post-dynamic recrystallization mechanism. The model assumes that no concurrent static recrystallization takes place after deformation (i.e. no new nucleation after deformation). Low dislocation density grains grow at the expense of high dislocation density grains (deformed grains). A fully recrystallized microstructure can then be reached within times as short as a few minutes (example shown in Fig. 6). At this stage, the evolution is mainly controlled by the difference of stored energy between the growing grains and the surrounding material.

The evolution of dislocation density in post-dynamic regime is described by:

$$\frac{\partial \rho}{\partial t} = -K_s\,(T)\,.\rho \tag{7}$$

where K_s is the static recovery parameter.

The identification of post-dynamically recrystallized grains is based on their dislocations density via the GOS parameter.

4. Numerical simulation

4.1. Identification of model parameters

To be able to model the DDRX, 4 parameters must be identified:

$$\left\{K_1\,(\dot{\varepsilon})\,;K_2\,(\dot{\varepsilon}.T)\,;K_3\,(\dot{\varepsilon},\,T)\,;K_g(\dot{\varepsilon},\,T)\right\}.$$

Therefore recrystallization kinetics was experimentally investigated under different thermomechanical conditions. The numerical parameters were identified based on the values of recrystallized fraction and recrystallized grain size measured by EBSD technique, and shown in Figs. 7 and 8.

The parameters identified for the dynamic regime are the same as those used for the post-dynamic evolutions except for the grain boundary mobility which could possibly be different under static conditions. The new value was determined based on the evolution of grain size during static annealing at high temperatures (Fig. 9).

Table 2. Thermomechanical conditions of the study.

Temperature (°C)	1000	1010	1020	1030	1050	1080
Strain rate (s^{-1})	0.03	0.05	0.1	0.05	0.1	0.1

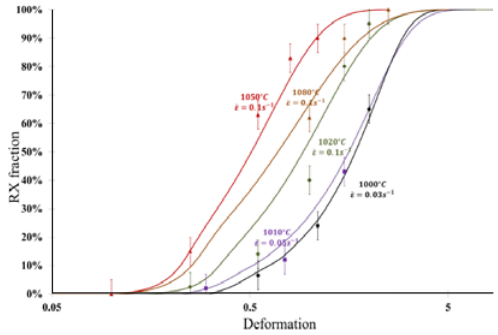

Figure 7. Evolution of recrystallized fraction as a function of deformation, for different thermomechanical conditions.

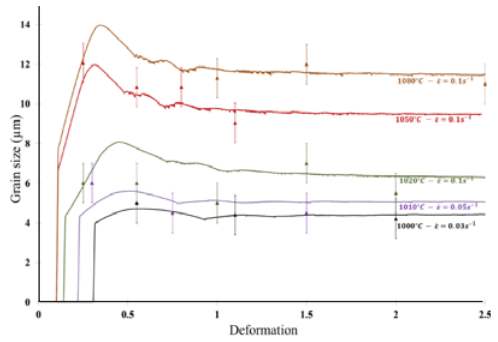

Figure 8. Evolution of recrystallized grain size as a function of deformation, for different thermomechanical conditions.

The mobility is estimated by the following equation [11]:

$$M = \frac{M_0}{T}.\exp\left(\frac{-Q_M}{RT}\right) \tag{8}$$

where M_0 is the pre-exponential constant and Q_M is the activation energy. Based on our experimental results (Fig. 9), Q_M is estimated to 426 kJ/mol.

4.2. Variation of model parameters

In order to be able to calculate the model parameters for other thermomechanical conditions without doing further experiments, and in order to check the physical relevance of the parameters variations, the Zener-Hollomon parameter was introduced:

$$Z = \dot{\varepsilon}.\exp\left(\frac{Q}{RT}\right) \tag{9}$$

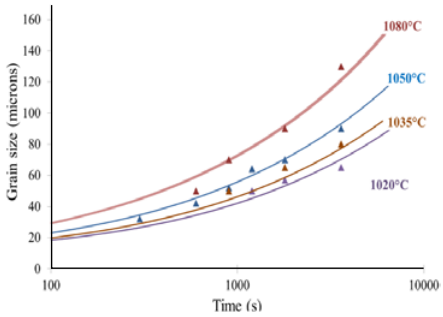

Figure 9. Grain size evolution during static annealing in the δ-solvus domain.

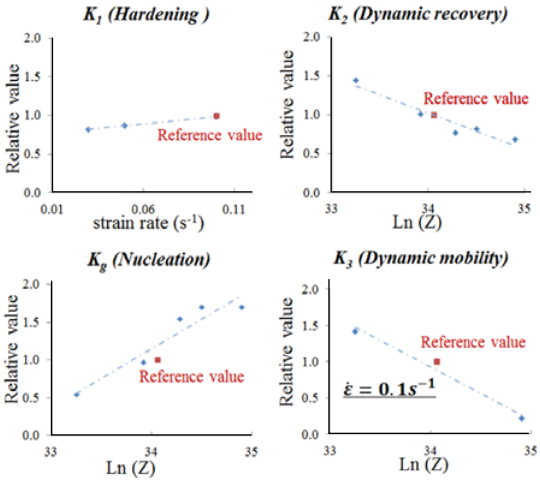

Figure 10. Evolution of the model parameters as a function of the thermomechanical conditions.

where $\dot{\varepsilon}$ is the strain rate, T the temperature and Q the activation energy set in this study to 400 kJ/mol for Inconel 718 [1].

4.2.1. Dynamic evolution

The variation of the model parameters with the Zener-Hollomon parameter is investigated in dynamic conditions (Fig. 10). Parameters identified at 1050 °C for a strain rate of $0.1s^{-1}$ are taken as a reference, and the other parameters are expressed in a dimensionless form relative to the reference values.

Increasing the temperature for a constant strain rate results in faster kinetics and larger recrystallized grain size. The parameters K_2 (dynamic recovery) and K_3 (dynamic mobility) increase while K_g (nucleation probability) decreases, which is physically consistent. The hardening parameter K_1 is assumed to be only sensitive to the variation of strain rate.

For a constant temperature, when the strain rate increases, the hardening is more important and the dynamic recovery is more difficult. An increase in the nucleation probability is observed and results in faster recrystallization kinetics with smaller grain size. These observations are also physically consistent.

The dynamic mobility increases with both temperature and strain rate. The strain rate dependency may be related to vacancies concentration, which affects the grain

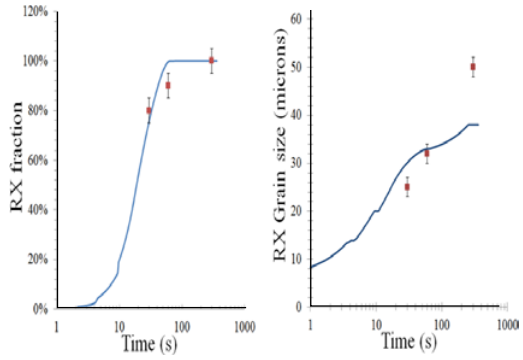

Figure 11. Post-dynamic recrystallization kinetics after deformation at 1050 °C to ε =0.55, $\dot{\varepsilon} = 0.1\ s^{-1}$.

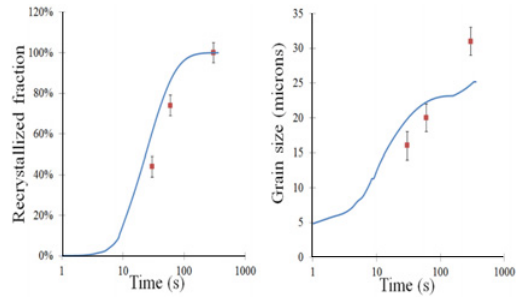

Figure 12. Post-dynamic recrystallization kinetics after deformation at 1010 °C to ε =0.55, $\dot{\varepsilon} = 0.05\ s^{-1}$.

boundary velocities. The variation of K_3 can be described by a law close to the Arrhenius type:

$$K_3 = \frac{K_{3\_0}}{T}.\exp\left(\frac{Q(\dot{\varepsilon})}{RT}\right). \quad (10)$$

4.2.2. Post-dynamic evolution

During the dynamic regime, as the material deforms, the dislocation density of RX grains increases until it reaches a steady-state value. When the deformation stops, microstructural observations reveal the presence of three categories of grains: NR grains, deformed RX grains and newly nucleated RX grains. The deformed RX grains are, on a microstructure point of view, close to the NR grains. Actually, the dislocation density difference between the last nucleated grains and the rest of the deformed RX and NR grains is so important that it outbalances the capillarity forces and controls the evolution of the microstructure at the beginning of the post-dynamic regime. Therefore, at the beginning of the post-dynamic regime, the microstructure is reclassified, based on the dislocation density values. A low dislocation density threshold is set at the beginning of the simulation to separate RX from NR grains. Grains having lower dislocation density than the threshold value keep being considered as recrystallized grains. Those with higher dislocation density (including NR but also some of the former RX grains) are classified as non-recrystallized grains.

The same parameters identified in dynamic regime are used for the simulation of post-dynamic recrystallization.

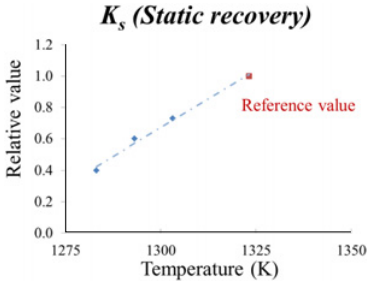

Figure 13. Evolution static recovery parameter as a function of the temperature.

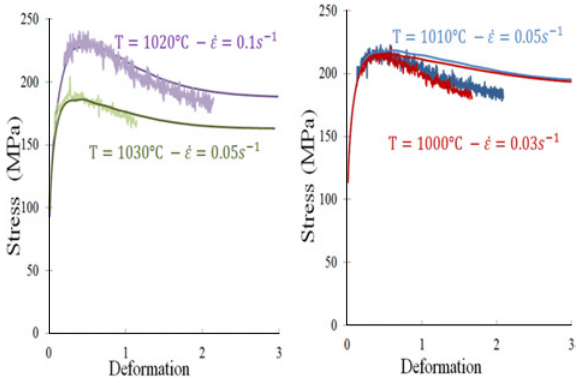

Figure 14. Comparison between experimental and numerical stress-strain curves.

The identification of the static recovery parameter was done based on experimental data (Fig. 13).

The numerical simulation of recrystallization kinetics presented in Fig. 11 and Fig. 12 show a good agreement with the experimental data.

It is important to mention that simulation results presented above were obtained in only a few minutes.

4.2.3. Mechanical behavior

Based on the evolution of dislocation density of the representative grain i (Eq. (1)), the flow stress is calculated with the Taylor equation [7]:

$$\sigma_i = \sigma_0 + \alpha\,\mu \mathrm{Mb}\sqrt{\rho_i} \qquad (11)$$

where μ is the shear modulus, b the Burgers vector, M the Taylor factor, α a constant set to 0.2, and σ_0 a "dislocation free" yield stress.

The comparison between experimental and numerical stress-strain curves showed a good agreement, as shown in Fig. 14.

At the beginning of deformation, the mechanical behavior is mainly controlled by hardening mechanisms. The onset of recrystallization and the nucleation of new "dislocation-free grains" result in a softening in the curve. The competition between hardening and softening leads to a steady-state where the stress remains constant with increasing strain.

The mismatch between the experimental and numerical curves at 1000 °C and 1010 °C is probably due to the self-heating of the material during deformation. At high temperature and low strain rate, the deformation can be considered as isothermal. When the strain rate decreases or when the temperature decreases, the amount of self-heating can no longer be neglected, since it induces significant softening.

5. Conclusion

The evolution of recrystallization kinetics, recrystallized grain size, and mechanical behavior during hot forging of Inconel 718 were investigated in this work. A previously published two-site mean field model allowed to predict the recrystallized fraction, the grain size distribution and the strain-stress curves during dynamic and post-dynamic recrystallization. A good agreement between the numerical simulation and the experimental data was observed. The model requires the identification of 4 parameters for the dynamic regime, and a fifth one to account for post-dynamic evolutions.

For now, the model parameters were identified for different thermomechanical conditions in the δ-Supersolvus domain. The variation of the model parameters with the Zener-Hollomon parameter allow to simulate the nucleation for variable thermomechanical conditions.

Ongoing work extends the present study to the δ-subsolvus domain. Interactions, sometimes very complex, between different physical phenomena have then to be described and taken into account in the model.

This work has been supported by Forges de Bologne. The authors are very grateful the MSR technical staff members for their support in performing experiments.

References

[1] S. C Medeiros, Y. V. R. K Prasad, W. G Frazier, R Srinivasan , Mater Sci Eng A, **293**, 198-207 (2000)
[2] H.-T. Lee e, W.-H. Hou, Mater Sci Eng A, **555**, 13–20 (2012)
[3] D. S. Weaver, S. L. Semiatin, Scripta Mater A. **57**, 1044-1047 (2007)
[4] H. Yuan, W.C. Liu, Mat. Sc. And Eng., **408**, 281-289 (2005)
[5] A.A Guimaraes and J.J Jonas, Met. Trans., **12A**, 1655-1666 (1981)
[6] L.X. Zhou, T. N. Baker, Mater. Sci. Eng, **A 196**, 89–95 (1995)
[7] P. Bernard, S. Bag, K. Huang, and R. E. Loge, Mater Sci Eng A, **528**, 7357–7367 (2011)
[8] N.K. Park, I.S. Kim, Y.S. Na, J.T. Yeom, J. of Mat. Proc. Tec., **111**,98-102 (2001)
[9] J. De Jaeger, D.Solas, T. Baudin, O. Fandeur, , J.-H. Schmitt, C. Rey in Superalloys 201, John Wiley & Sons, Inc., Hoboken, NJ, USA (2012)
[10] F. Montheillet, O. Lurdos, and G. Damamme, Acta Mater., **57**,1602–1612 (2009)
[11] F.J. Humphreys and M. Hatherly, "Recrystallization and related annealing phenomena", Elsevier Ltd Second Edition (2004)